

# Enhanced Computational Sampling of Perylene and Perylothiophene Packing with Rigid-Body Models - Supplementary Information

Evan D. Miller<sup>†</sup>, Matthew L. Jones<sup>†</sup>, and Eric Jankowski<sup>†,\*</sup>

<sup>†</sup>*Micron School of Materials Science and Engineering, Boise State University, 1910 West  
University Dr., Boise, Idaho 83725, United States*

E-mail: ericjankowski@boisestate.edu

## Contents

S1 Determination of Equilibrium	S3
S2 Molecular Dynamics Force Field and Computing Infrastructure	S4
S3 Omission of Electrostatic Calculations	S6
S4 Unit Conversions	S7
S5 Determination of $\xi$ Cut Off	S10
S6 Distribution of $\theta$	S11
S7 System Size Comparison	S12
S8 Checkerboard-Aligned Energies	S13
S9 Performance Comparisons	S14
S9.1 TPS . . . . .	S15
S9.1.1 Disordered Phase . . . . .	S15
S9.1.2 Ordered Phase . . . . .	S16
S9.1.3 Eclipsed Phase . . . . .	S17

S9.2	Potential Energy . . . . .	S18
S9.2.1	Disordered Phase . . . . .	S18
	S9.2.1.1 Relaxation Time . . . . .	S18
	S9.2.1.2 Autocorrelation . . . . .	S19
S9.2.2	Ordered Phase . . . . .	S20
	S9.2.2.1 Relaxation Time . . . . .	S20
	S9.2.2.2 Autocorrelation . . . . .	S21
S9.2.3	Eclipsed Phase . . . . .	S22
	S9.2.3.1 Relaxation Time . . . . .	S22
	S9.2.3.2 Autocorrelation . . . . .	S23
S9.3	Order Parameter, $\psi$ . . . . .	S24
S9.3.1	Disordered Phase . . . . .	S24
	S9.3.1.1 Relaxation Time . . . . .	S24
	S9.3.1.2 Autocorrelation . . . . .	S25
S9.3.2	Ordered Phase . . . . .	S26
	S9.3.2.1 Relaxation Time . . . . .	S26
	S9.3.2.2 Autocorrelation . . . . .	S27
S9.3.3	Eclipsed Phase . . . . .	S28
	S9.3.3.1 Relaxation Time . . . . .	S28
	S9.3.3.2 Autocorrelation . . . . .	S29

**References**

**S29**

## S1 Determination of Equilibrium

The potential energy can be used to measure when a morphology has reached equilibrium by determining when its evolution becomes constant as a function of time ( $dE/dt = 0$ ). The calculation is accomplished by separating the total potential energy for each timestep into 10 equally sized bins. The average and standard deviation over each bin is calculated and compared to the average and standard deviation of the final bin. When the average potential energy of a bin is within the standard deviation of the final bin, the energy is no longer changing and the system is considered to have reached equilibrium. In the example shown in Figure S1, the red line indicates the critical point  $\tau_r$  beyond which the average value of the potential energy is shown to be within one standard deviation of the potential energy of the final bin.  $\tau_r$  therefore represents the timestep at which equilibrium has occurred.

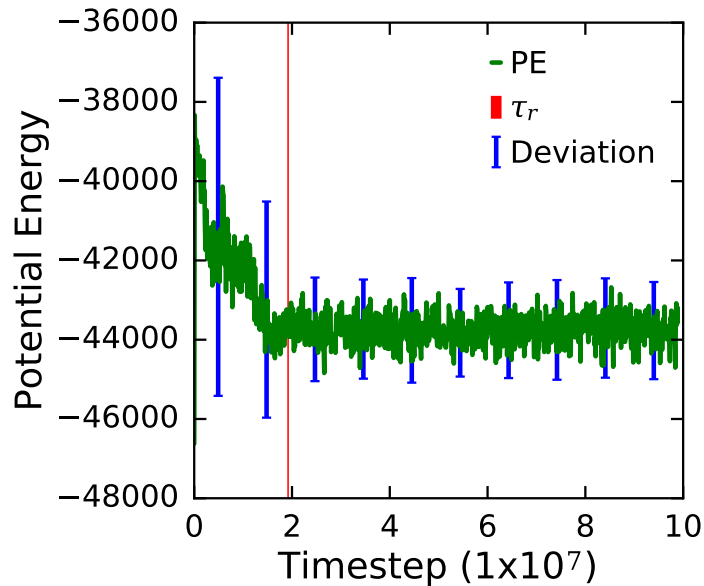


Figure S1: Potential energy as a function of increasing timestep (green). The standard deviation for each bin is shown in blue. The red vertical line is the timestep at which the system is considered relaxed.

## S2 Molecular Dynamics Force Field and Computing Infrastructure

For this investigation, the Optimized Potential for Liquid Simulations (OPLS) Force Field is used.<sup>1</sup> The atomic masses are defined as  $M_C = 12.01$  amu and  $M_S = 32.06$  amu. The masses of the hydrogen atoms are not considered during the molecular dynamics simulations themselves, but are taken into account as  $M_H = 1.00$  amu in the density calculations. The constants used in the force field for the two molecules are defined in Table S1-Table S5. Note that, in the interest of computational efficiency, all carbon united atoms in the simulation are treated as C-H groups, and so the atom type ‘C’ describes the diatomic species.

The simulations leverage the Kestrel and Maverick supercomputers at Boise State University (BSU) and the Texas Advanced Computing Center (TACC) respectively, using a single NVIDIA K40 graphics processing unit (GPU) per simulation at TACC and a single NVIDIA K20 GPU per simulation at BSU.

Table S1: Non-bonded interaction parameters used in the MD simulations. Heterogeneous atom pair interactions  $\sigma_{ij} = \sqrt{\sigma_i\sigma_j}$  and  $\epsilon_{ij} = \sqrt{\epsilon_i\epsilon_j}$ . Pair interactions are defined by a Lennard-Jones potential:  $U_{pair}(r) = 4\epsilon \left[ \left(\frac{\sigma}{r}\right)^{12} - \left(\frac{\sigma}{r}\right)^6 \right]$ .

Atom Type	$\sigma$ (Å)	$\epsilon$ (kcal mol <sup>-1</sup> )
C	3.8	0.122
S	3.5	0.359

Table S2: Bond-stretching parameters used in the MD simulations. Bonds are defined by the following potential:  $U_{bond}(r) = k_b(r - r_0)^2$ . Note that bond equilibrium distances  $r_0$  are given in terms of the carbon atom diameter  $\sigma_C$ .

Bond Type	$r_0$ (Å)	$k_b$ (kcal mol <sup>-1</sup> Å <sup>-2</sup> )
Perylene		
C-C	1.52	253.5
Perylothiophene		
C-C	1.52	745.8
C-S	1.71	745.8

Table S3: Angle-bending parameters used in the MD simulations. Angles are defined by the following potential:  $U_{angle}(\theta) = k_a(\theta - \theta_0)^2$ .

Angle Type	$\theta_0$ (rad)	$k_a$ (kcal mol <sup>-1</sup> rad <sup>-2</sup> )
Perylene		
C-C-C	2.09	46.36
Perylothiophene		
C-C-C	2.09	136.42
C-C-S	2.09	136.42
C-S-C	1.60	136.42

Table S4: Torsional parameters used in the MD simulations. Torsions are defined by the following potential:  $U_{dihedral}(\phi) = \frac{1}{2}k_1(1 + \cos(\phi)) + \frac{1}{2}k_2(1 - \cos(2\phi)) + \frac{1}{2}k_3(1 + \cos(3\phi)) + \frac{1}{2}k_4(1 - \cos(4\phi))$ .

Dihedral Type	$k_1$ (kcal mol <sup>-1</sup> )	$k_2$ (kcal mol <sup>-1</sup> )	$k_3$ (kcal mol <sup>-1</sup> )	$k_4$ (kcal mol <sup>-1</sup> )
Perylene				
C-C-C-C	0.00	6.10	0.00	0.00
Perylothiophene				
C-C-C-C	0.00	17.95	0.00	0.00
C-C-C-S	0.00	17.95	0.00	0.00
C-C-S-C	0.00	17.95	0.00	0.00
C-S-C-C	0.00	17.95	0.00	0.00

Table S5: Improper torsional parameters used in the MD simulations. Improper torsions are defined by the following potential:  $U_{improper}(\chi) = k_i(\chi - \chi_0)^2$ .

Improper Type	$\chi_0$ (rad)	$k_i$ (kcal mol <sup>-1</sup> rad <sup>-2</sup> )
Perylene		
C-C-C-C	0.00	1.22
Perylothiophene		
C-C-C-C	0.00	3.59
C-C-C-S	0.00	3.59
C-C-S-C	0.00	3.59
C-S-C-C	0.00	3.59

### S3 Omission of Electrostatic Calculations

The goal of this paper is to highlight how high-throughput MD can be used to quickly generate phase behavior of planar aromatic systems and provide comparisons to experimental work. In it, we omit electrostatic interactions between partially charged atoms in order to reduce the number of required calculations and allow for higher-throughput in this work. As an example, preliminary simulations of perylene conducted with partial atomic charges and their electrostatic interactions showed an average of 273.44 time steps per second whereas simulations excluding the electrostatic interactions averaged 1434.69 time steps per second. Therefore, we are able to increase the speed of the calculations by 3-4 $\times$  by omitting the electrostatic forces.

We see that the omission of charges likely leads to differences in packing angle compared to what is typically seen in planar aromatic molecules.<sup>2</sup> For instance, the work of Tsuzuki et al. has shown, using quantum chemical calculations applied to dimers of thiophene-based molecules, that these electrostatic interactions perform a crucial role in favoring the perpendicular orientations observed in herringbone structures.<sup>3</sup> It could therefore be expected that the bulk structural behavior of perylene and perylothiophene would be similarly affected, leading to the herringbone structures observed in the  $\alpha$ -polymorphs. We note, however, that the diffraction patterns for these systems obtained in this investigation are in good agreement with those obtained experimentally, and so, for a bulk material, a charge neutral model appears to describe the most important physics required to obtain realistic morphological structures at a wide variety of state points. It is therefore left to the reader to decide whether the computational benefit of omitting the electrostatic charge calculations will outweigh the small-scale differences in packing information for their own systems.

## S4 Unit Conversions

In the HOOMD-blue simulation suite<sup>4-6</sup> unitless temperatures are related to real temperatures by the equation:

$$T_{SI} = \frac{T_{unitless} * \epsilon}{k_B} \quad (1)$$

where  $T_{SI}$  is the physical temperature in kelvin,  $T_{unitless}$  is the unitless temperature,  $\epsilon$  is the energy scale factor (0.122 and 0.359 kcal mol<sup>-1</sup> for perylene and peryloothiophene respectively), and  $k_B$  is the Boltzmann constant. The values obtained for  $T_{real}$  are presented below in Table S6.

Table S6: The simulation temperature with the corresponding actual temperature in Kelvin for Perylene and Perylothiophene.

$T_{unitless}$	$T_{SI}$ , Perylene (K)	$T_{SI}$ , Perylothiophene (K)
1	61.25	180.16
2	122.49	360.33
3	183.74	540.49
4	244.98	720.65
5	306.23	900.81
6	367.47	1080.98
7	428.72	1261.14
8	489.96	1441.30
9	551.21	1621.46
10	612.45	1801.63
11	673.70	1981.79
12	734.94	2161.95
13	796.19	2342.11
14	857.43	2522.28
15	918.68	2702.44
16	979.92	2882.60
17	1041.17	3062.76
18	1102.41	3242.93
19	1163.66	3423.09
20	1224.90	3603.25
21	1286.15	3783.41
22	1347.39	3963.58
23	1408.64	4143.74
24	1469.89	4323.90
25	1531.13	4504.07
26	1592.38	4684.23
27	1653.62	4864.39
28	1714.87	5044.55
29	1776.11	5224.72
30	1837.36	5404.88

Densities are calculated by:

$$\rho = \frac{N * M_w}{V}, \quad (2)$$

where  $N$  is the number of molecules,  $M_w$  is the molecular weight, and  $V$  is the simulation volume. Densities values investigated are presented below in Table S7.

Table S7: Densities in  $\text{g}/\text{cm}^3$  at which the calculations were conducted.

Perylene ( $\text{g}/\text{cm}^3$ )	Perylothiophene ( $\text{g}/\text{cm}^3$ )
0.01	0.01
0.12	0.13
0.37	0.39
0.61	0.65
0.85	0.91
1.04	1.11
1.22	1.30
1.40	1.50
1.59	1.69
1.77	1.89

## S5 Determination of $\xi$ Cut Off

As perylene and perylothiophene are annealed, intracolumnar order increases due to intermolecular attractive forces surpassing thermal vibrations. This leads to the formation of an eclipsed phase in which the perylene/perylthiophene molecule covers the one behind it. To measure when this phase emerges, the  $\xi$  values are measured over the complete range of temperatures tested. It is observed that  $\xi$  converges to  $\sim 0.95$  as temperature is lowered, for all  $\rho$  (Figure S2). The  $\xi$  cut-off value is taken as 0.90 to allow for fluctuations in  $\xi$ .

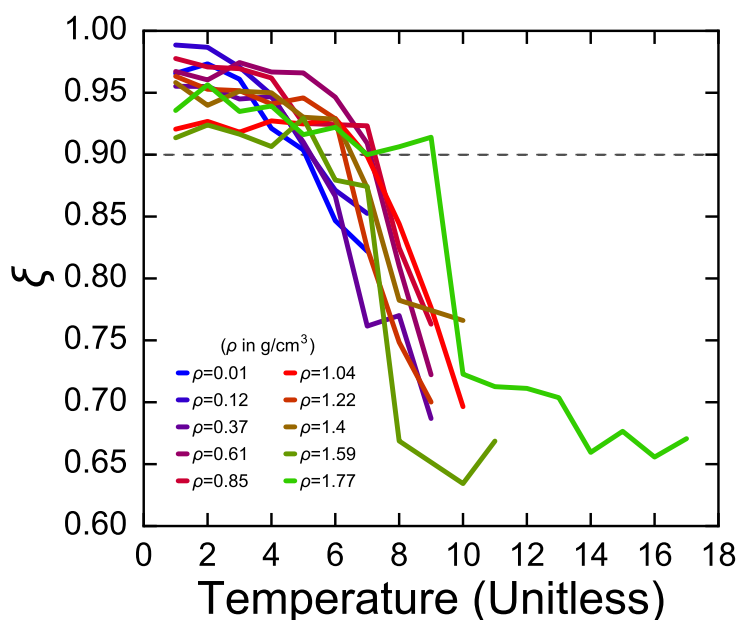


Figure S2: As temperatures decrease, the degree of eclipsing ( $\xi$ ) for all  $\rho$  measured converge to  $\sim 0.95$ . The horizontal dashed black line is considered the cut off for a system to be considered in the eclipsed phase.

## S6 Distribution of $\theta$

The cut off of the dot product of 0.96 is chosen from the distribution of the dot product values. The distribution of dot product values for the system shown in Figure 2 in the text is shown in Figure S3b. The dot product reaches a maximum at 1 and if an angle is  $\pm 16^\circ$  the dot product will still be 0.96. Therefore, we assume the distribution of values is symmetric around one, and split our distribution across one accordingly (as shown in Figure S3b). We then fit a Gaussian curve to the dot product distribution. We find that at  $\sigma = 4.5$  that the dot product value is 0.96.

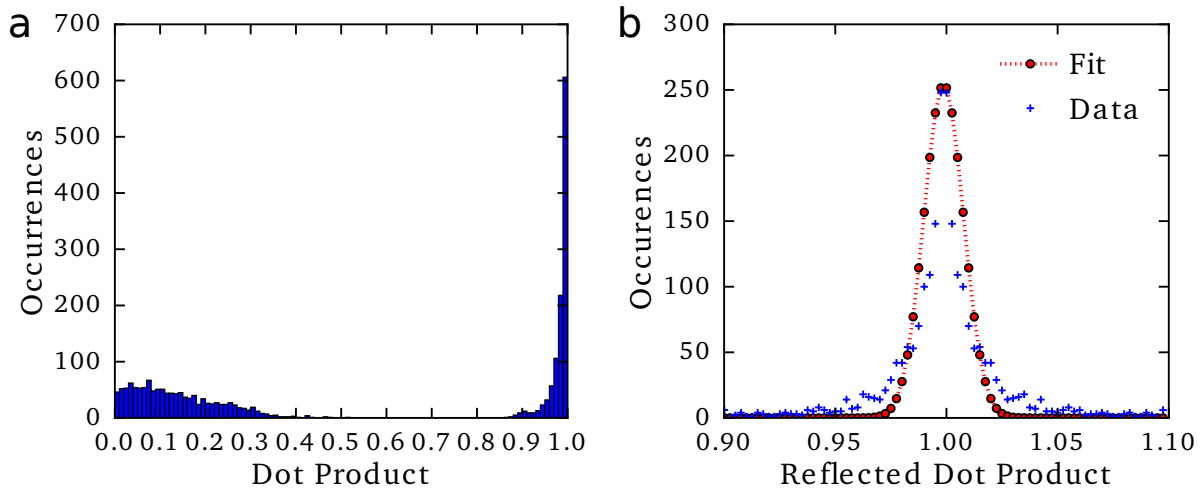


Figure S3: (a) Histogram of dot product values in the ordered system shown in the text Figure 2. (b) Dot product values approximated to a Gaussian curve. We find that the dot product equals 0.96 at a  $\sigma$  of 4.5.

## S7 System Size Comparison

Simulations are run with 200 to 1500 molecules. Figure S4a and b show that both systems relax to the energetically favored, hexagonally-packed columns. Both systems are also shown to be very ordered by visual inspection (Figure S4a,b). Due to the structural similarities (including a near indistinguishable radial distribution function as shown in Figure S4c), only the more computationally efficient simulations of 200 molecules are considered for further analysis in the main text.

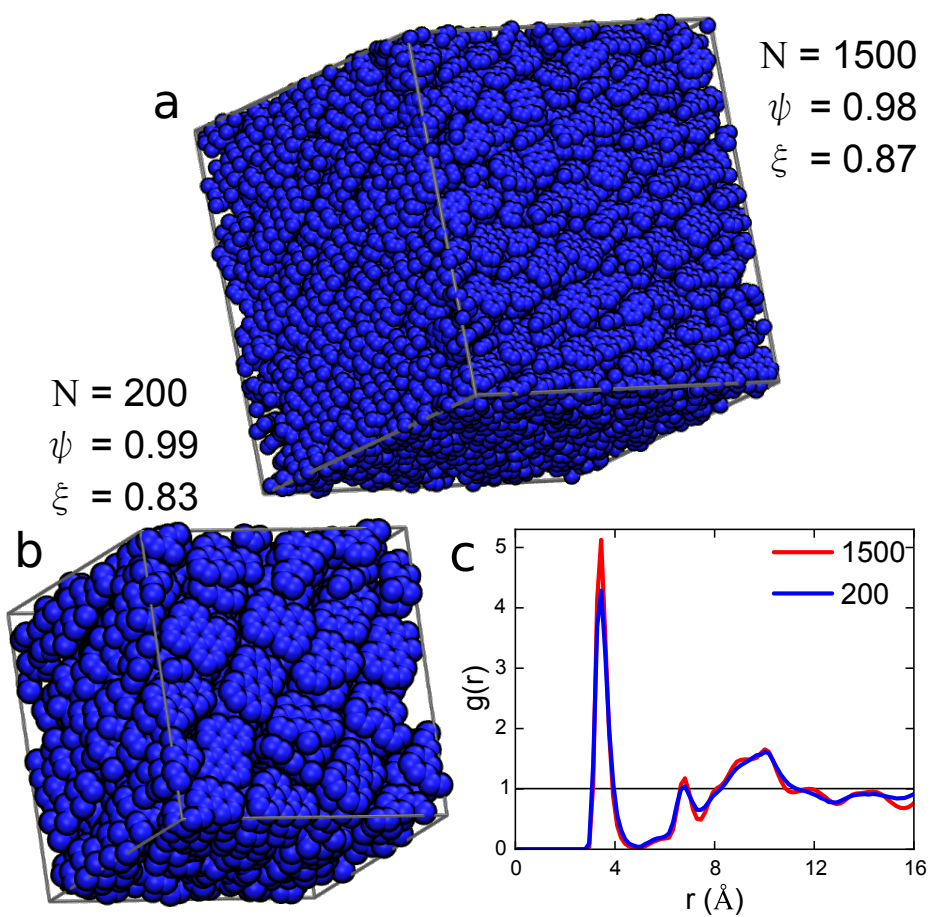


Figure S4: Example morphologies and calculated  $\xi$  and  $\psi$  values for (a)  $N = 1500$  and (b)  $N = 200$  molecule systems. (c) The comparison of the radial distribution function.

## S8 Checkerboard-Aligned Energies

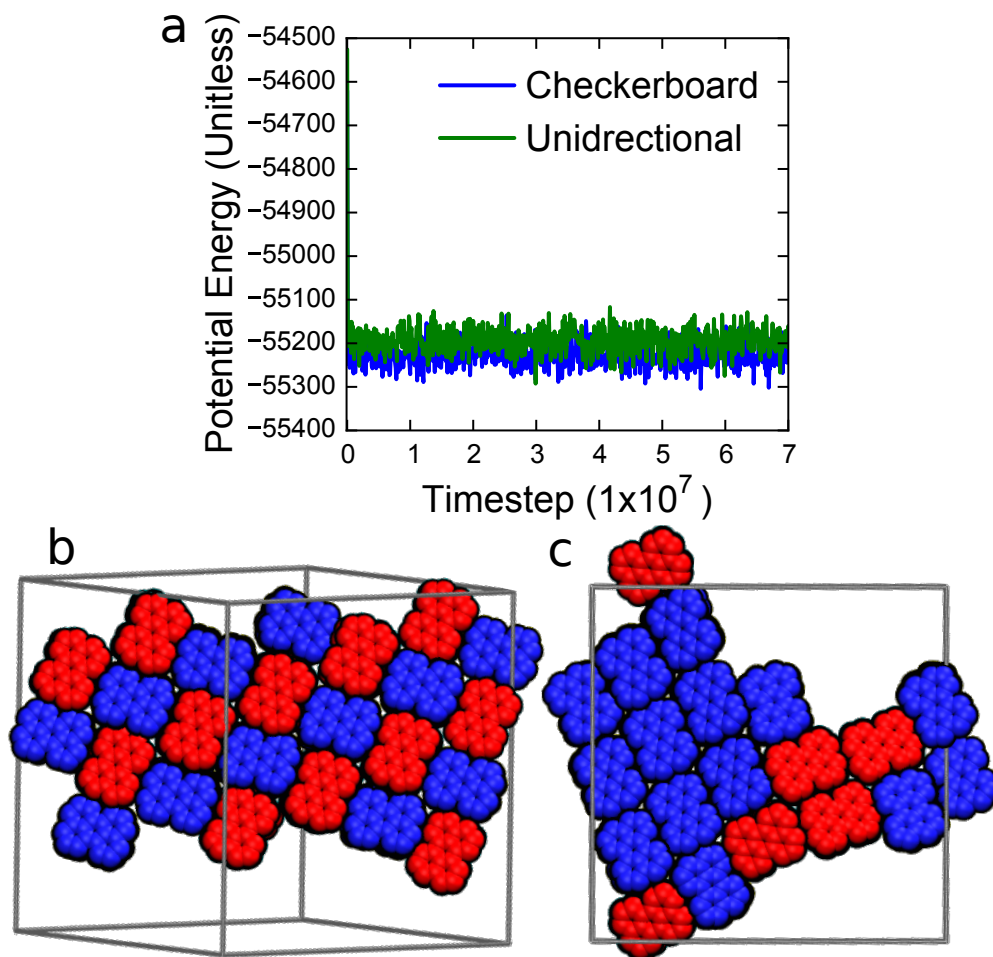


Figure S5: (a) Potential energies of the two structures showing significant overlap of the potential energies in the (b) checkerboard structure and (c) aligned structure.

The potential energies of the checkerboard and aligned structural motifs are found to be nearly equal (Figure S5a). The checkerboard morphology (Figure S5b) has a potential energy of  $-55226 \pm 34$  whereas the aligned system (Figure S5c) has a potential energy of  $-55193 \pm 37$  (the plus/minus is the standard deviation). The morphologies shown in Figure S5 are simulations of rigid perylene conducted at  $\rho = 1.22 \text{ g/cm}^3$ . The runs were executed for 12 hours at  $T = 10$  ( $\sim 600 \text{ K}$ ), then the temperature was lowered in  $\Delta T$  increments of 1 ( $\sim 60 \text{ K}$ ) to the final temperature:  $T = 60 \text{ K}$ . The only difference between the two runs is the initial configuration.

## S9 Performance Comparisons

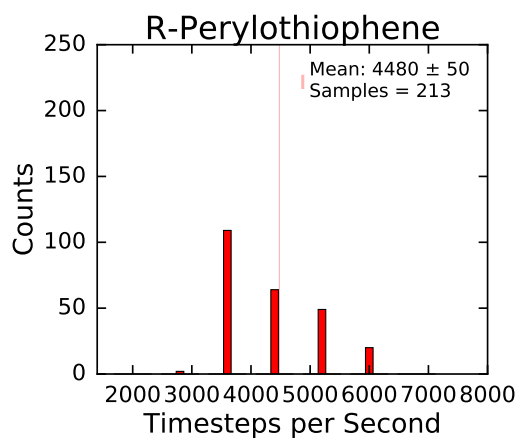
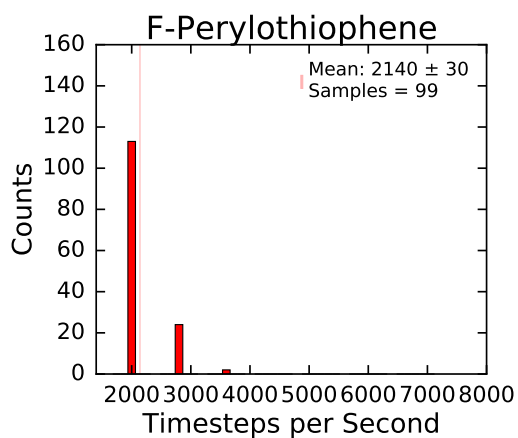
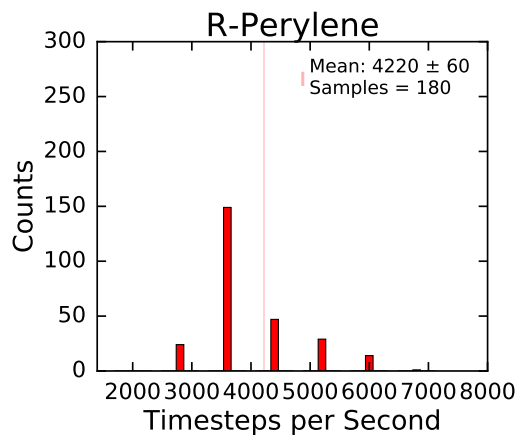
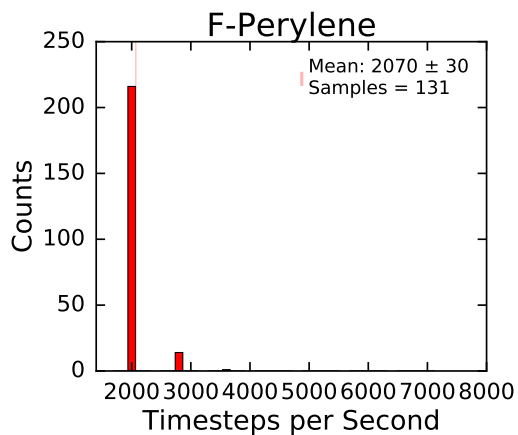
We use three parameters to compare and contrast the performance in our four systems: time steps per second, Lennard-Jones potential energy, and the order parameter. The process for obtaining the order parameter is explained in the text, and here, we calculated the order parameter for each snapshot. Using the method shown in section S1, we determine the frames required to reach equilibrium based off of Lennard-Jones energy and order parameter then determine the number of snapshots required for independent frames using the autocorrelation function. These results are normalized in the text as direct comparison between models becomes most clear when relaxation and autocorrelation times are normalized by the time steps per second. Below are presented histograms with unnormalized mean values and standard errors of the three parameters, along with the total number of samples considered for each system. Also included are the number of samples considered in these mean and deviation calculations. Histograms are calculated separately for each phase and by both energy and order metrics.

The wall-clock time for each simulation can be calculated by dividing the number of time steps required to equilibrate or structurally decorrelate by the TPS of that system. For instance, in the ordered case, the flexible perylene system took, on average, around 70 minutes of wall-clock time to relax and produced a statistically independent structure every 27 minutes thereafter. Rigid perylene, on the other hand, relaxed in around 44 minutes and produced a new independent structure every 18 minutes. Flexible perylothiophene equilibrated in just under 1 hour, with an autocorrelation time of a further 27 minutes. Finally, rigid perylothiophene reach relaxation in 42 minutes, taking a further 20 minutes to produce stastically independent samples.

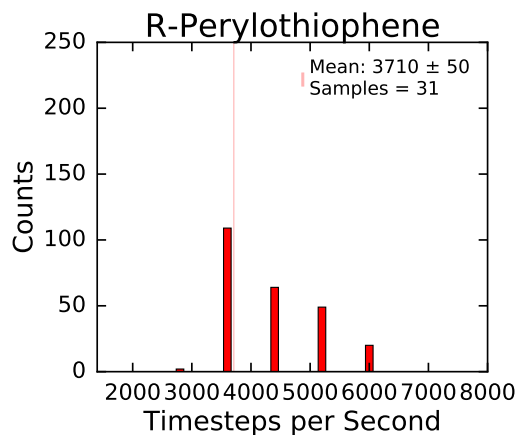
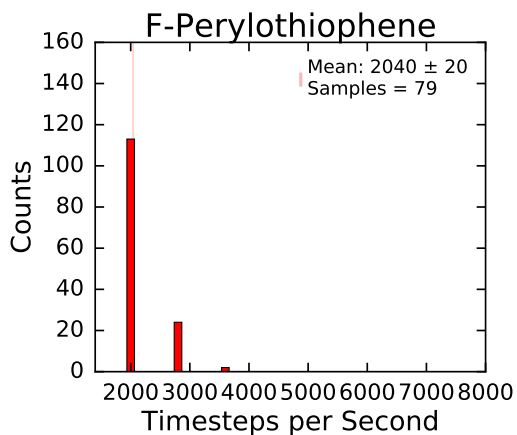
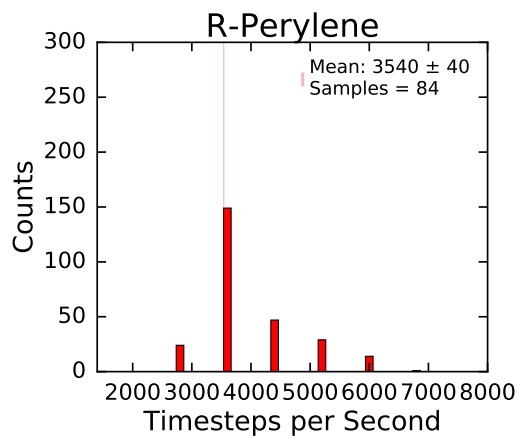
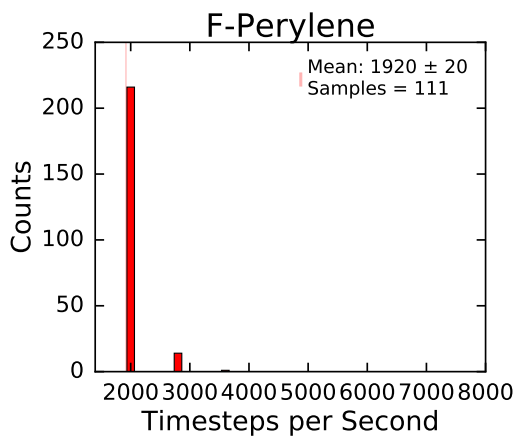
Note that the ordered simulations were performed on different computing hardware (NVIDIA K40 GPUs) to the disordered and eclipsed simulations (NVIDIA K20 GPUs), so the time steps per second between phases do not necessarily compare.

## S9.1 TPS

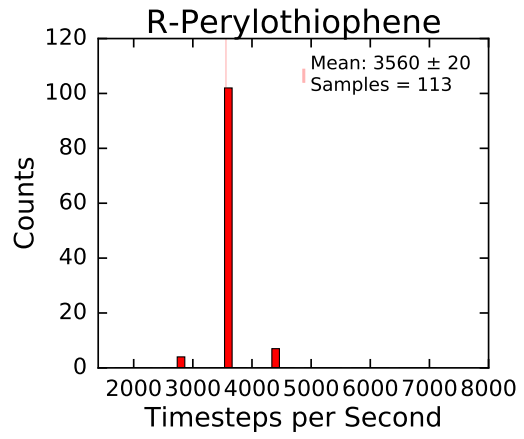
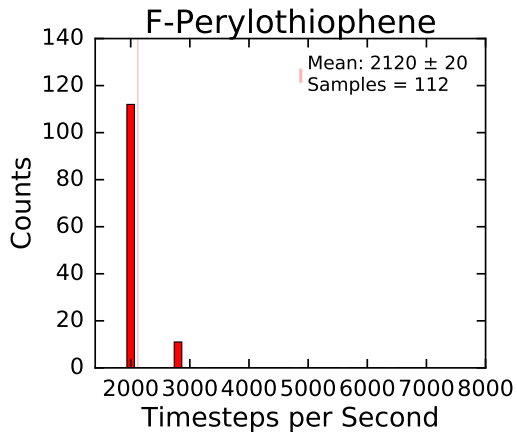
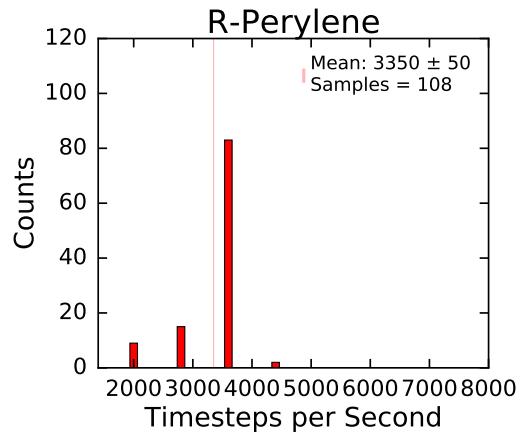
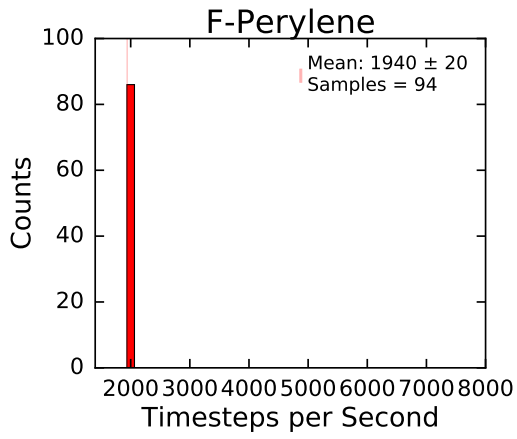
### S9.1.1 Disordered Phase



### S9.1.2 Ordered Phase



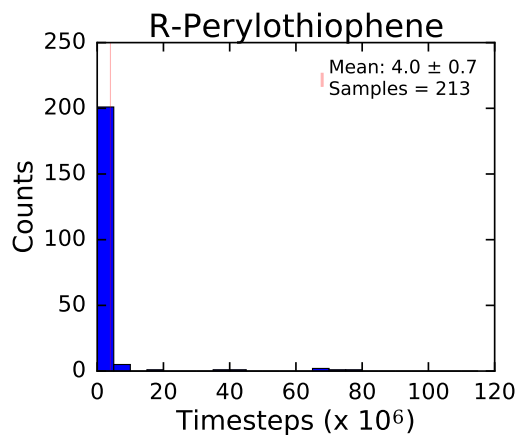
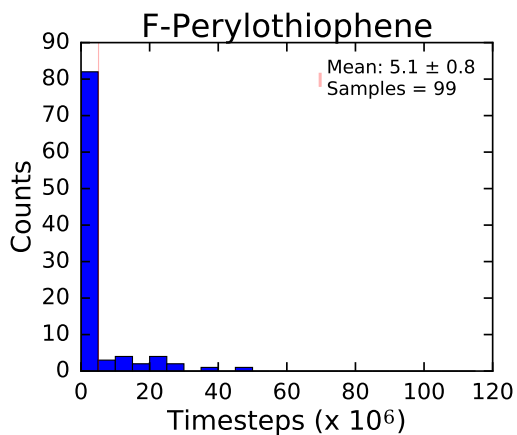
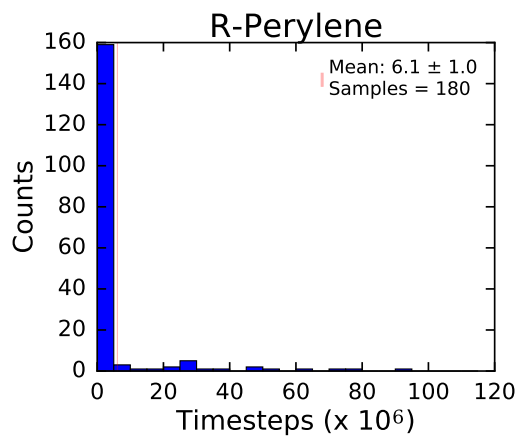
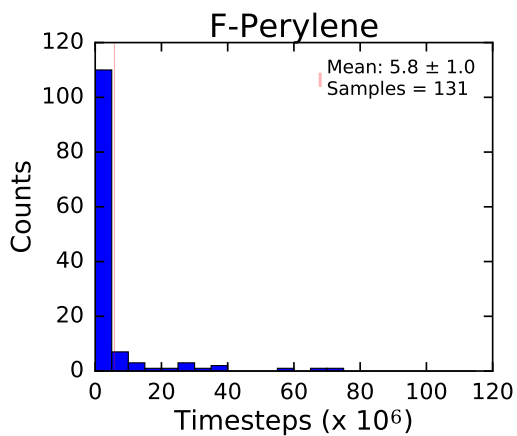
### S9.1.3 Eclipsed Phase



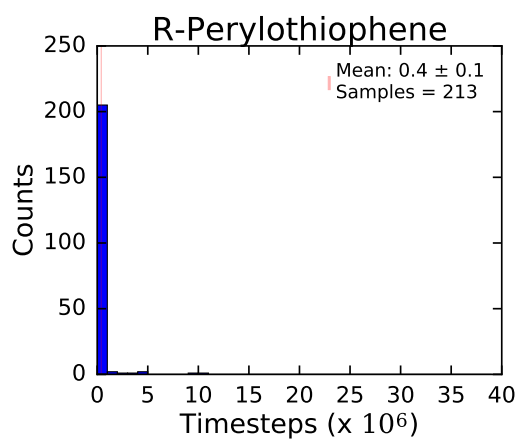
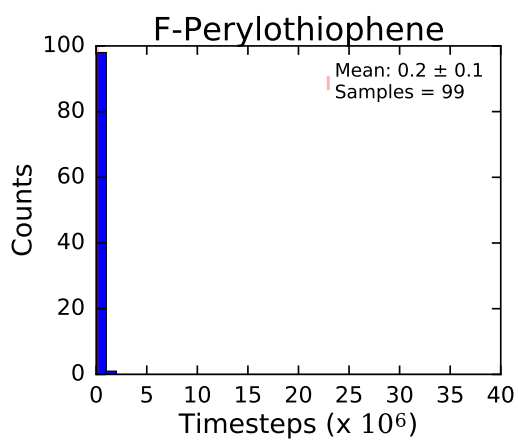
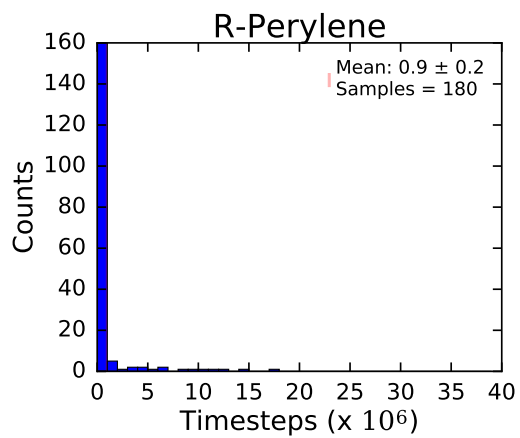
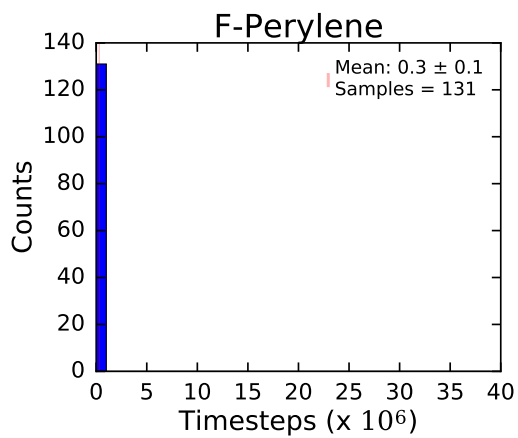
## S9.2 Potential Energy

### S9.2.1 Disordered Phase

#### S9.2.1.1 Relaxation Time

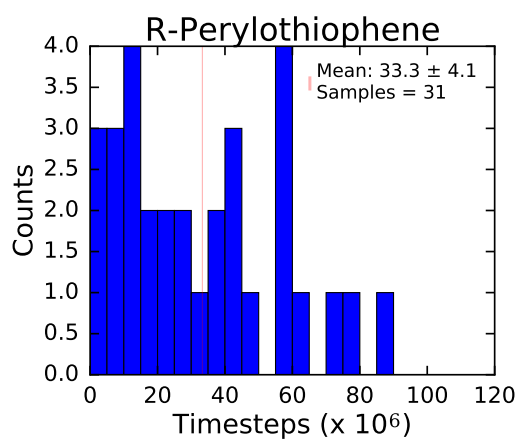
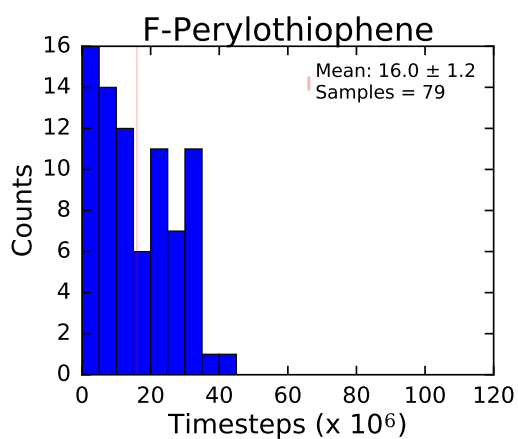
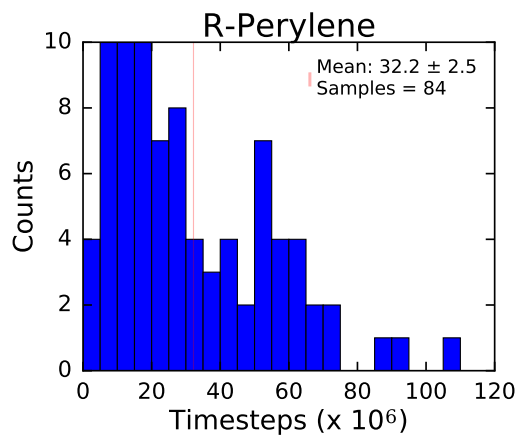
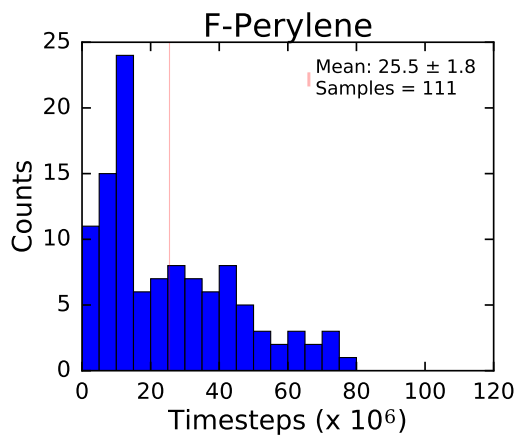


### S9.2.1.2 Autocorrelation

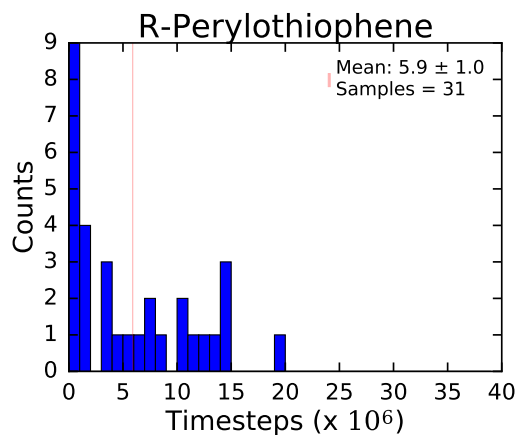
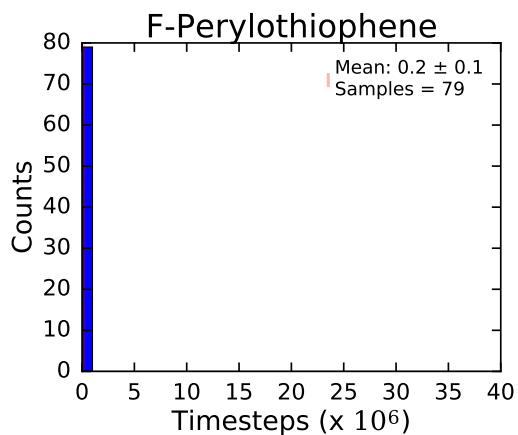
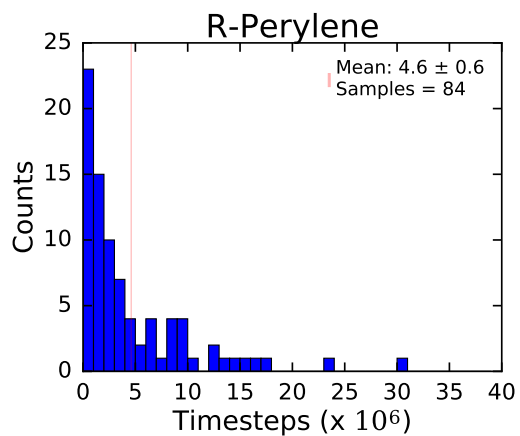
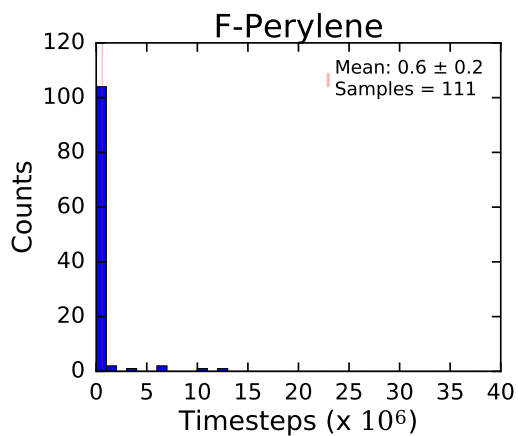


## S9.2.2 Ordered Phase

### S9.2.2.1 Relaxation Time

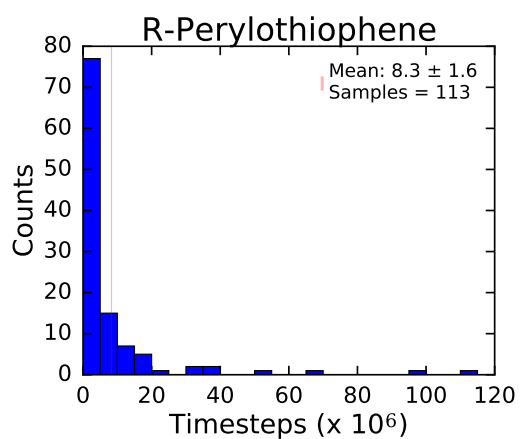
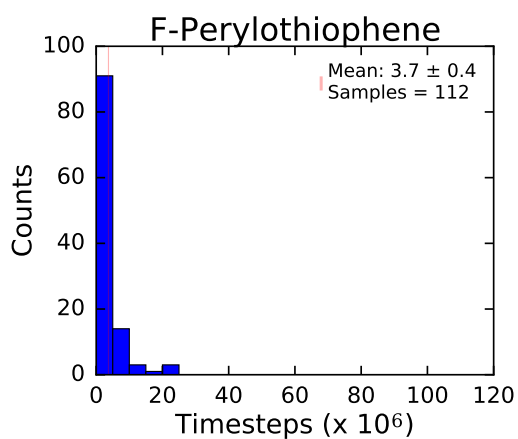
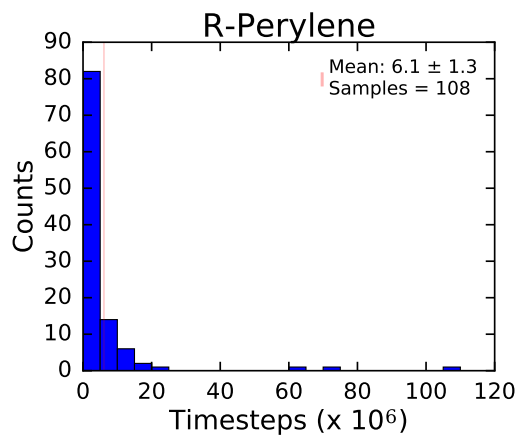
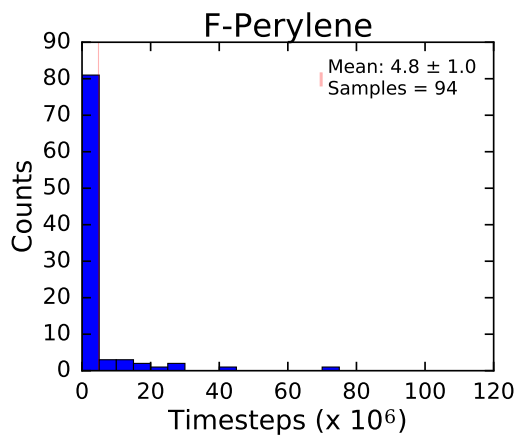


### S9.2.2.2 Autocorrelation

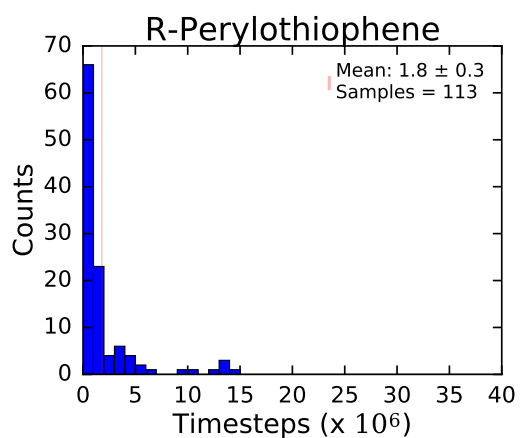
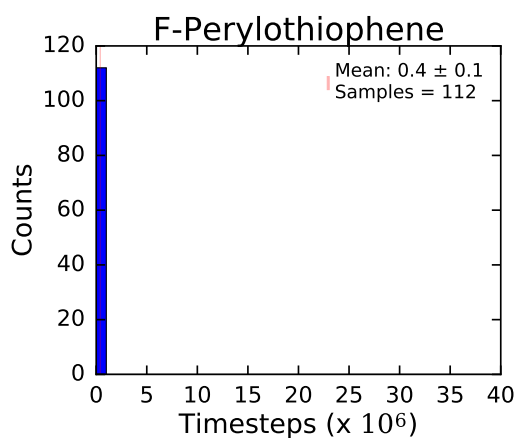
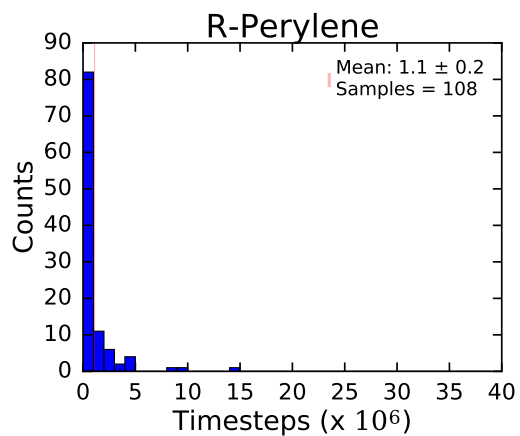
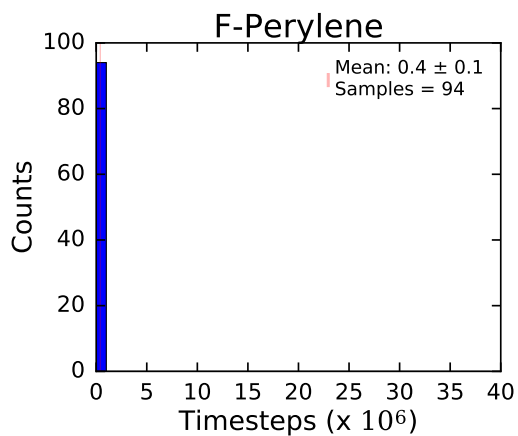


## S9.2.3 Eclipsed Phase

### S9.2.3.1 Relaxation Time



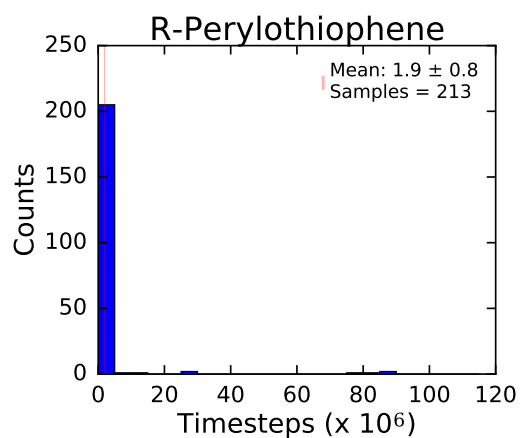
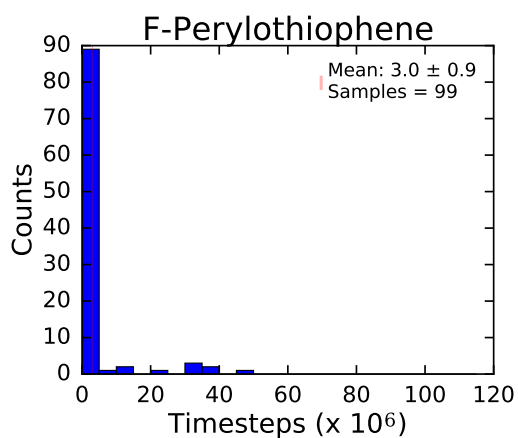
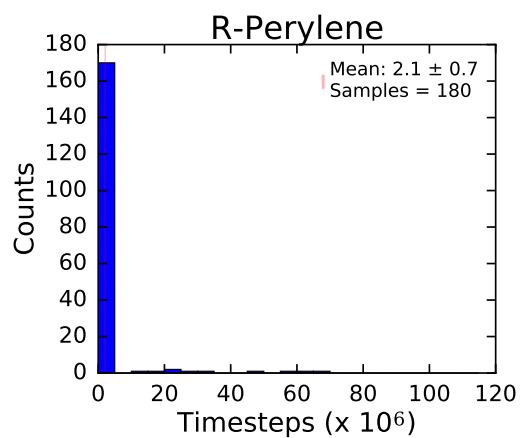
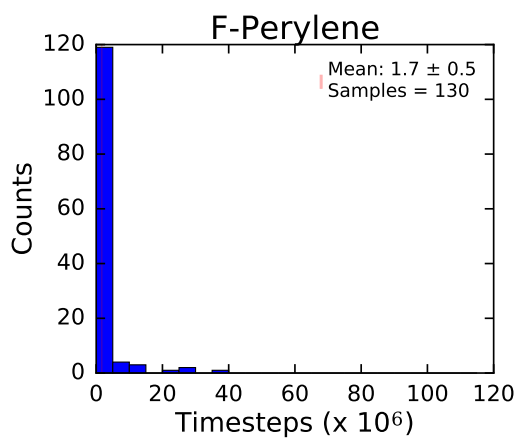
### S9.2.3.2 Autocorrelation



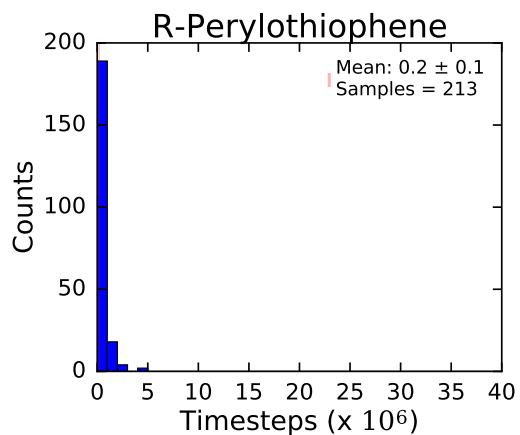
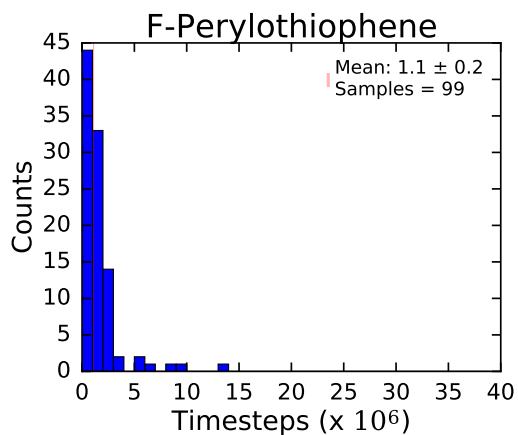
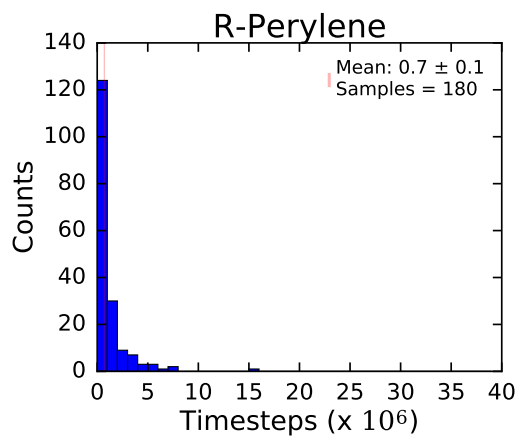
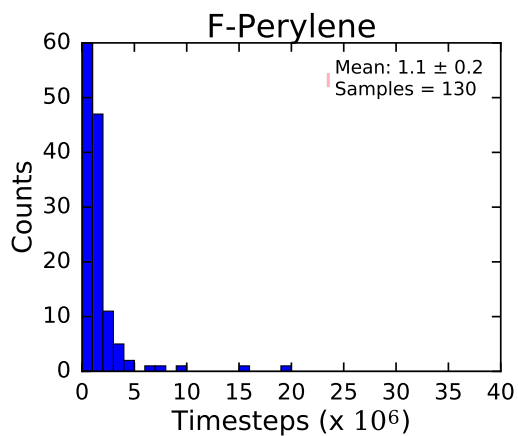
## S9.3 Order Parameter, $\psi$

### S9.3.1 Disordered Phase

#### S9.3.1.1 Relaxation Time

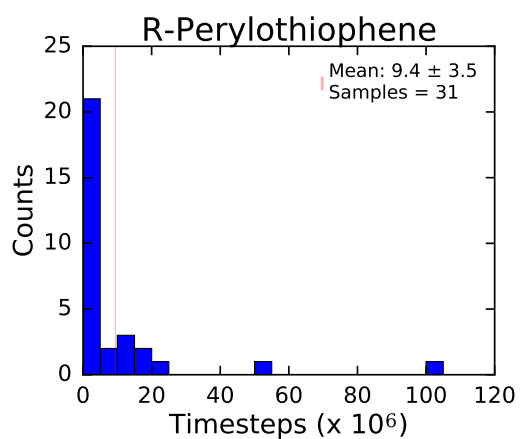
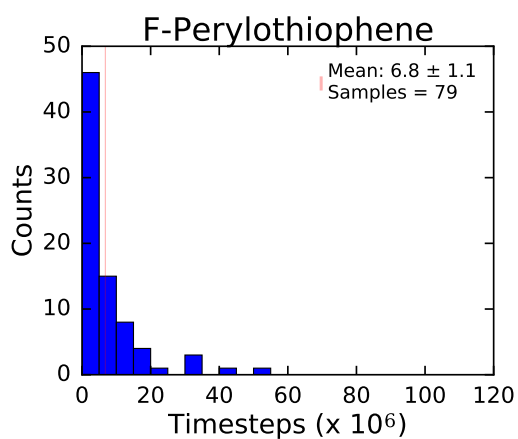
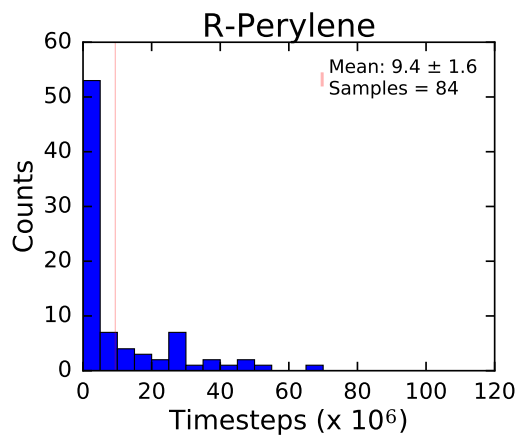
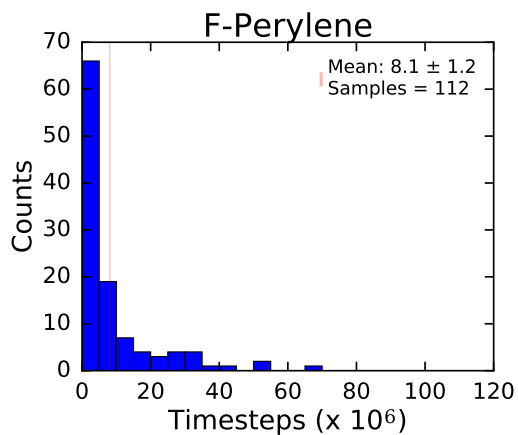


### S9.3.1.2 Autocorrelation

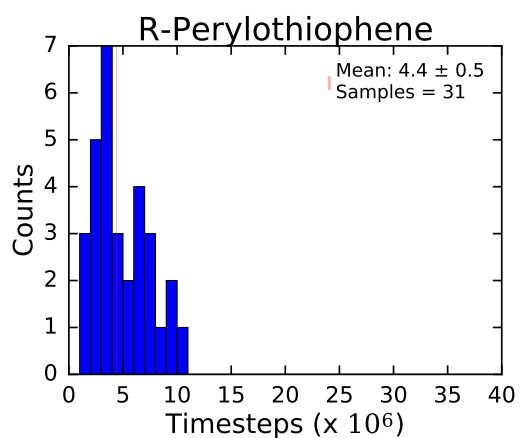
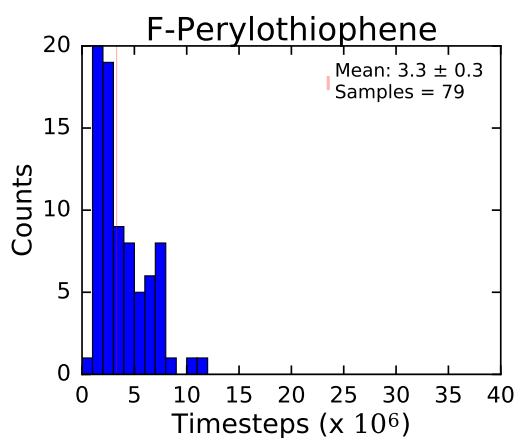
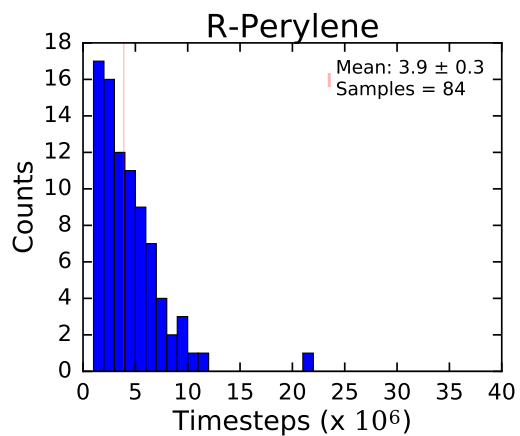
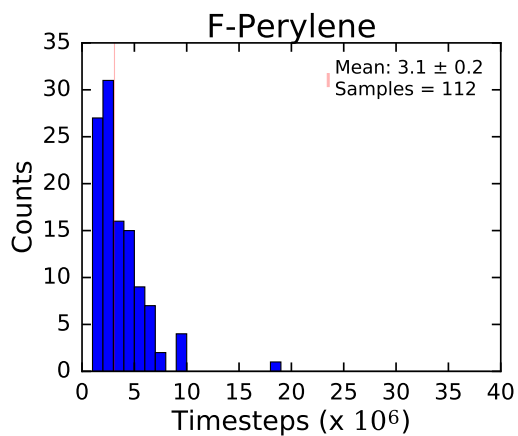


## S9.3.2 Ordered Phase

### S9.3.2.1 Relaxation Time

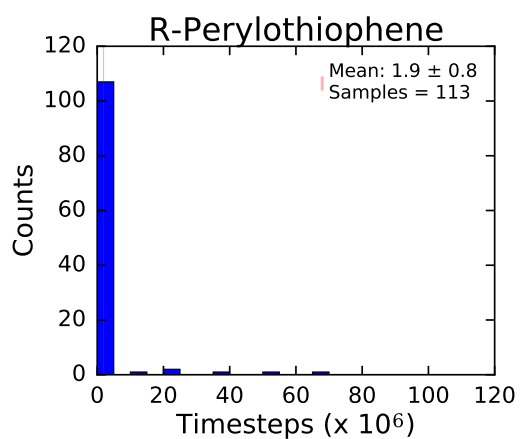
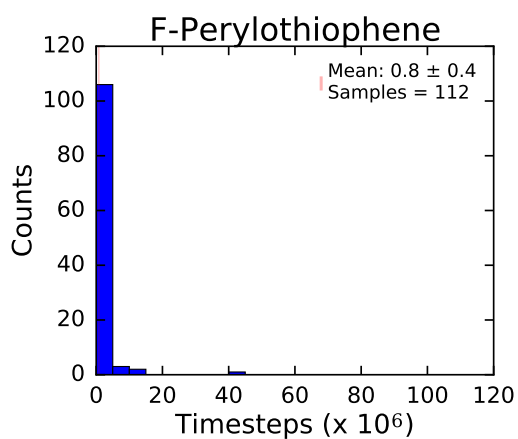
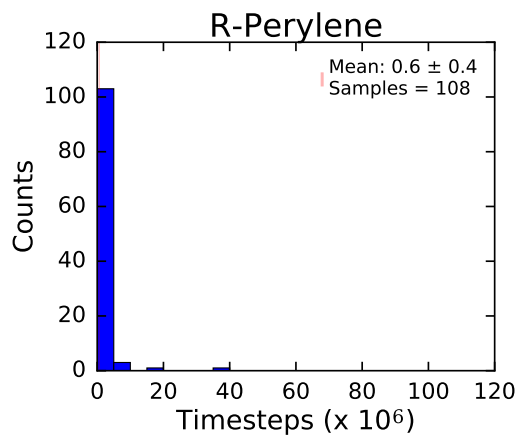
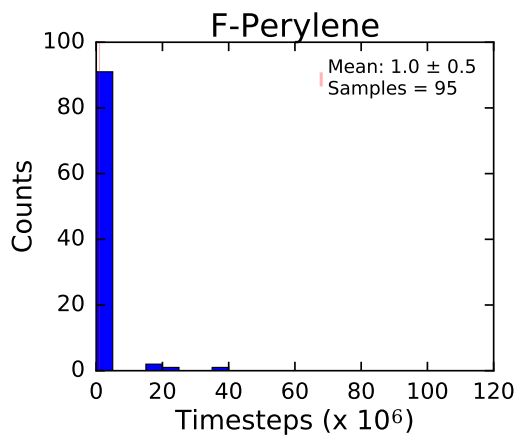


### S9.3.2.2 Autocorrelation



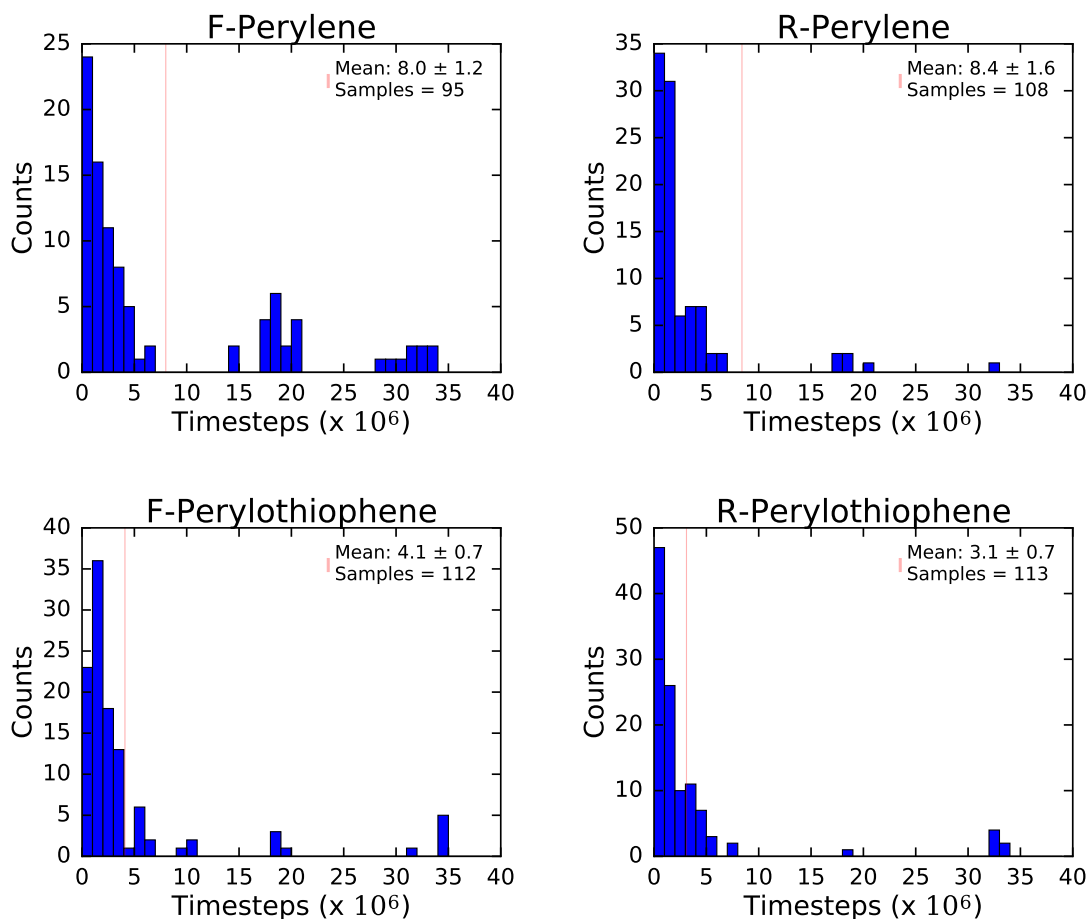
### S9.3.3 Eclipsed Phase

#### S9.3.3.1 Relaxation Time



Note: these systems are initialized from a higher-temperature organized conformation. Therefore, the relaxation times are negligible.

### S9.3.3.2 Autocorrelation



## References

- (1) Jorgensen, W. L.; Tirado-Rives, J. *Journal of the American Chemical Society* **1988**, *110*, 1657–1666.
- (2) Desiraju, G. R.; Gavezzotti, A. *Acta Crystallographica Section B* **1989**, *45*, 473–482.
- (3) Tsuzuki, S.; Honda, K.; Azumi, R. *Journal of the American Chemical Society* **2002**, *124*, 12200–12209.
- (4) Anderson, J. A.; Lorenz, C. D.; Travesset, A. *Journal of Computational Physics* **2008**, *227*, 5342–5359.
- (5) Glaser, J.; Nguyen, T. D.; Anderson, J. A.; Lui, P.; Spiga, F.; Millan, J. A.; Morse, D. C.; Glotzer, S. C. *Computer Physics Communications* **2014**, *192*, 97–107.
- (6) HOOMD-blue web page. <http://codeblue.umich.edu/hoomd-blue>.